THE JOURNAL OF PHYSICAL CHEMISTRY B

pubs.acs.org/JPCB Article

Direct Evidence That Mutations within Dysferlin's C2A Domain Inhibit Lipid Clustering

Thaddeus W. Golbek, Shauna C. Otto, Steven J. Roeters, Tobias Weidner, Colin P. Johnson,* and Joe E. Baio*

Cite This: J. Phys. Chem. B 2021, 125, 148–157 Read Online

ACCESS | Metrics & More | Article Recommendations | Supporting Information

ABSTRACT: Mechanical stress on sarcolemma can create small tears in the muscle cell membrane. Within the sarcolemma resides the multidomain dysferlin protein. Mutations in this protein render it unable to repair the sarcolemma and have been linked to muscular dystrophy. A key step in dysferlin-regulated repair is the binding of the C2A domain to the lipid membrane upon increased intracellular calcium. Mutations mapped to this domain cause loss of binding ability of the C2A domain. There is a crucial need to understand the geometry of dysferlin C2A at a membrane interface as well as cell membrane lipid reorientation when compared to that of a mutant. Here, we describe a comparison between the wild-type dysferlin C2A and a mutation to the conserved aspartic acids in the domain binding loops. To identify both the geometry and the cell membrane lipid reorientation, we applied sum frequency generation (SFG) vibrational spectroscopy and coupled it with simulated SFG spectra to observe and quantify the interaction with a model cell membrane composed of phosphotidylserine and phosphotidylcholine. Observed changes in surface pressure demonstrate that calcium-bridged electrostatic interactions govern the initial interaction of the C2A domains docking with a lipid membrane. SFG spectra taken from the amide-I region for the wild type and variant contain features near 1642, 1663, and 1675 cm^{-1} related to the C2A domain β-sandwich secondary structure, indicating that the domain binds in a specific orientation. Mapping simulated SFG spectra to the experimentally collected spectra indicated that both wild-type and variant domains have nearly the same orientation to the membrane surface. However, examining the ordering of the lipids that make up a model membrane using SFG, we find that the wild type clusters the lipids as seen by the increase in the ratio of the CD_3 and CD_2 symmetric intensities by 170% for the wild type and by 120% for the variant. This study highlights the capabilities of SFG to probe with great detail biological mutations in proteins at cell membrane interfaces.

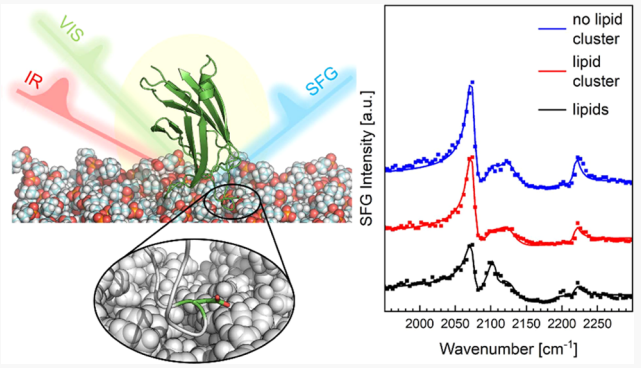

INTRODUCTION

The movement required by daily life places stress on the sarcolemma creating small tears in the muscle cell membrane.[1−3] Repair of the membrane depends on a multidomain protein termed dysferlin.[4,5] Mutations in dysferlin render it unable to reseal the tears in the muscle cell membrane and result in recessive forms of muscular dystrophy including limb-girdle muscular dystrophy, Mioshi myopathy, and distal anterior compartment myopathy.[3,4,6−8]

Dysferlin is a 237 kDa protein composed of a transmembrane domain at the C-terminus and seven C2 domains. The N-terminus, in response to intracellular calcium, binds to lipids and repairs tears on the sarcolemmal membrane.[2,4,6] These C2 domains are linked together in tandem, with the C2A domain furthest from the transmembrane domain.[9,10] C2 domains are typically composed of an eight-stranded β-sandwich fold and represent one of the largest families of proteins including synaptotagmins, protein kinases, DOC2, and ferlins.[11,12] Within the C2 domains are lipid and calcium binding loops that contain acidic residues.[6,13] It is believed that C2 domains target the protein to a membrane surface based on the membrane lipid composition such that the loops on one edge of the domain make electrostatic contact, have hydrophobic interactions, and dock with a lipid surface.[14] The docking of the binding loops can cause lipid clustering and spontaneous curvature change of the membrane, which facilitates membrane fusion and exocytosis.[15−19]

It has been suggested that dysferlin facilitates the resealing of muscle cell membrane tears by vesicle fusion.[13,20,21] There is some evidence that following the release of calcium, from a tear on the muscle cell membrane, the C2A domain of

Received: August 4, 2020
Revised: December 3, 2020
Published: December 23, 2020

https://dx.doi.org/10.1021/acs.jpcb.0c07143
J. Phys. Chem. B 2021, 125, 148–157

dysferlin binds to calcium and membranes, and then mediates the fusion of the vesicle with the muscle cell membrane.[4] It has also been demonstrated that mutations within the C2A domain of dysferlin disrupt this fusion process.[17,19] The C2A domain of dysferlin is 14 kDa with a β-sandwich structure with three aspartic acids in the proposed lipid binding loops.[2,17,19] Additionally, binding assays have demonstrated that dysferlin C2A binds to vesicle surfaces made up of variable anionic lipid compositions including 25% anionic and 75% zwitterionic.[2,17,19,22] This domain has been shown to have calcium binding sensitivity, and previous studies of mutations to the aspartic acid residues have shown a loss of calcium binding sensitivity.[17] Also, previous work with binding assays has shown that mutations to this domain inhibit the binding ability to lipid vesicles.[19] This set of previous binding assays provides the relative amount of protein bound to vesicles and demonstrates the need for calcium to dock. Thus, we wish to specifically focus on how mutations to the C2A domain directly affect the protein docking ability and vesicle structural changes that occur during the first step in vesicle fusion after the release of calcium.

To identify the specific interactions between dysferlin C2A domain and lipids, we characterized the protein−lipid binding interface with sum frequency generation (SFG).[23] SFG is a second-order nonlinear optical technique capable of detecting biomolecule adsorption and orientation at interfaces.[24−28] The technique involves a fixed visible laser that is pulsed in temporal and spatial synchronicity with a tunable infrared laser. SFG photons created by nonlinear optical frequency mixing carry a vibrational spectrum of the interfacial species. This technique is commonly used to study the packing and ordering of lipid monolayers at air/water interfaces.[29−35] Additionally, vibrations stemming from the amide groups within the backbone of a protein specify the secondary structure, while vibrations of the lipid monolayer provide a snapshot of lipid ordering before and after protein binding.[29] Overall, SFG provides a label-free method to study the protein adsorption, docking, and ordering at a model cell membrane.

In this study, we wish to observe how mutations within dysferlin C2A domain wild type (DYSwt) affect how the protein adsorbs and binds to a lipid interface. SFG experiments can be repeated for a variant of DYSwt that exhibits a loss of binding and calcium sensitivity, compared the DYSwt experiments.[17] This variant includes a substitution of an aspartic acid, at the proposed lipid binding loop, to an alanine (D16A).[29,31,32,36−45] The calcium binding activity of the C2A domain of dysferlin is critical to the protein's function. Either removal of the C2A domain or missense mutations that abrogate calcium binding of C2A result in loss of function for dysferlin. A previous study analyzed isothermal titration calorimetry data to identify three residues (D16, D21, and D71) that are essential for the calcium binding activity of the C2A domain.[17] Of these three aspartate residues, D16 was chosen for study because it is located in the middle of a disordered loop region of the domain. Missense mutations are therefore unlikely to perturb the tertiary fold of the domain. By contrast, D21 and D71 reside in areas of loops that are proximal to β strands, and thus, mutation may impact the domain structure. We therefore chose the D16A mutation to study the effect of loss of calcium binding due to the minimal perturbation of the fold of the domain.[2,17] However, we hypothesize that DYSwt will bind and dock with the lipids inserting the binding loops into the lipid headgroup clustering the lipids together, while the mutant, D16A, will bind in a similar orientation without clustering the lipids or inserting its binding loops into the lipid headgroups.

EXPERIMENTAL METHODS

Protein Construct and Purification. Human dysferlin cDNA (AF075575), a gift from Dr. Kate Bushby (Newcastle University), was used as a template for cloning. The C2A domain (amino acids 1−129: sequence in the Supporting Information (SI) section) was cloned into the pET-28a(+) vector (Novagen) between BamHI and HindIII restriction sites. Complementary flanking restriction sites for the dysferlin insert were generated by polymerase chain reaction (PCR) amplification using the following primers: forward 5′-GCG CGC GGA TCC ATG CTG AGG GTC TTC ATC CTC TAT GCC-3′ and reverse 5′-GCG CGC AAG CTT TTA AGC TCC AGG CAG CGG-3′. The D16A mutation was introduced using site-directed mutagenesis with the following primers: forward 5′-GCT GAT GTC GGT GGC GGG TGT GTG GAC-3′ and reverse 5′-GCT GAT GTC GGT GGC GGG TGT GTG GAC-3′.

BL21 DE3 cells harboring the expression plasmids were cultured overnight at 37 °C in Luria−Bertani broth containing 50 μg/mL kanamycin and 1% w/v glucose and were used to seed 1 L cultures of Luria−Bertani broth containing 50 μg/mL kanamycin at a ratio of 1:1000. These were then grown to an optical density of 0.6 at 37 °C and induced with 0.5 mM isopropyl β-D-1-thiogalactopyranoside (IPTG) for the wild-type construct and 0.1 mM IPTG for the D16A mutant. The protein was expressed for 16 h at 18 °C. Cultures were centrifuged at 4000 rpm at 4 °C for 20 min and resuspended in lysis buffer: 50 mM *N*-(2-hydroxyethyl)piperazine-*N*′-ethanesulfonic acid (HEPES) pH 8, 250 mM NaCl, 10% (v/v) glycerol, 5 mM $CaCl_2$, 1 mM phenylmethanesulfonyl fluoride (PMSF), and 1 μM leupeptin, pepstatin A, and aprotonin. Cells were lysed using a Microfluidics M-11P microfluidizer at 18 000 psi. CHAPS (0.5%, w/v) was added to the total lysate and left to rock for 1 h on ice.

Soluble fractions were then obtained by centrifugation in a Beckman J2-21 centrifuge at 20 000*g* at 4 °C for 20 min. The clarified lysate was bound to a HisPur Cobalt resin (Thermo Scientific) for 2 h with rocking at 4 °C. Beads were washed with 20 column volumes of lysis buffer, and the protein was eluted with 50 mM HEPES, 150 mM NaCl, 5 mM $CaCl_2$, and 200 mM imidazole. Purity of the elution fractions was confirmed by sodium dodecyl sulfate polyacrylamide gel electrophoresis (SDS-PAGE), pooled, and dialyzed against 50 mM HEPES, 150 mM NaCl, 5 mM $CaCl_2$, and 1 mM 1,4-dithiothreitol (DTT).

Lipid Interface Preparation. Within a Teflon trough, a lipid monolayer was assembled at the air−water interface. This trough contained approximately 10 mL of buffer (50 mM HEPES pH 7, 1 mM DTT, 150 mM NaCl, 1 mM $CaCl_2$) prepared with MilliQ water (Millipore Direct-Q3 System). Throughout all experiments, the surface pressure was monitored by a tensiometer (KSV NIMA with a Wilhelmy plate). The surface pressure was set to zero at the aqueous−air interface before the dropwise addition of phospholipids. The phospholipid 1,2-dipalmitoyl-d62-*sn*-glycero-3-[phospho-L-serine][sodium salt] (dDPPS, Avanti Polar Lipids, Inc.) was first dissolved in a 65:35:8 ratio of chloroform (HPLC grade, J.T. Baker), methanol (ACS grade, Fisher Chemical), and MQ water, respectively, and 1,2-dipalmitoyl-d62-*sn*-glycero-3-phos-

https://dx.doi.org/10.1021/acs.jpcb.0c07143
J. Phys. Chem. B 2021, 125, 148−157

phocholine (dDPPC, Avanti Polar Lipids, Inc.) was dissolved in chloroform. The lipids were then mixed to yield a 1:3 ratio of dDPPS and dDPPC lipids and then spread by dropwise addition to the aqueous surface via a Hamilton microsyringe until a surface pressure of approximately 12 mN/m was reached. A dysferlin C2A solution and its mutant D16A was injected into the aqueous subphase of the trough to reach a final concentration of 5 μM and allowed to interact for 4 h.

To calculate the binding geometry of each domain to the membrane surface normal, we had to calculate the relative number of proteins to lipids for each case. For the lipids, the surface pressure (Figure 1) recorded can be related by an isotherm to the mean molecular area.[35,46] For estimations of the amount of protein at the interface, it can be assumed that high protein concentration in the subphase contributes much more than the lipids to the final surface pressure.[47] Our amounts for the lipids are 1.6×10^{18} molecules per meter squared, the dysferlin C2A wild type is 1.4×10^{17} molecules per meter squared, and the D16A mutant is 3.2×10^{17} molecules per meter squared. We found that there is more protein at the surface for the case of the D16A than that of the DYSwt.

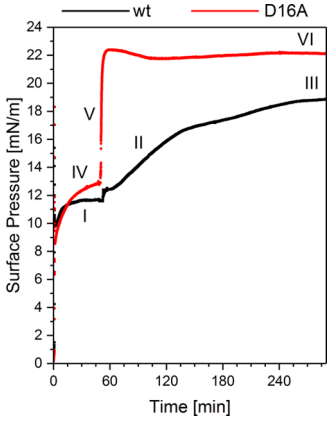

Figure 1. Graph shows the surface pressure versus time of wild type (wt, black) and D16A (red) adsorption to a 25% dDPPS and 75% dDPPC lipid monolayer. The lipid monolayer is formed (I and IV) at the air−water interface by the addition of lipids in chloroform until the desired pressure of approximately 11.7 mN/m for the wild type (wt) and approximately 12.7 mN/m for D16A mutant. After injection of wt (II) and D16A (V) into the subphase, the pressure is allowed to increase until equilibrium is reached. It took approximately 4 h for the wt (III) to reach pressure equilibrium with a value of 18.8 mN/m, while the D16A only took approximately 10 min (VI) with a value of 22.4 mN/m.

SFG Vibrational Spectroscopy. An EKSPLA Nd:YAG laser, operating at 50 Hz, was used to generate both a fixed visible (532 nm^{-1}) and tunable IR beam (1000−4000 cm^{-1}) via sequential pumping through an EKSPLA optical parametric generation/amplification and difference frequency unit, which utilized barium borate and $AgGaS_2$ crystals, respectively. The bandwidth was 2 cm^{-1} for the visible pump pulses and 4 cm^{-1} for the IR laser. The visible (~150 μJ/pulse) and IR beams (~200 μJ/pulse) were overlapped spatially and temporally at the desired interface, at incident angles of 60° and 54° versus the surface normal, to generate SFG photons, which were spectrally filtered, dispersed by a monochromator, and detected with a gated photomultiplier tube. Both beams were focused to an ~1 mm diameter at the interface. Spectra were collected in 4 cm^{-1} steps with 400 acquisitions per step. The SFG spectra were normalized by the product of the IR and visible pump beam intensities. The SFG spectrum was fit with the following equations[29,48,49]

$$I_{SFG} = |\chi^{(2)}_{eff}|^2 = \chi^{(2)}_{NR} + \chi^{(2)}_{surface} + \chi^{(3)} \quad (1)$$

where $\chi^{(2)}_{NR}$ and $\chi^{(2)}_{eff}$ are the nonresonant and off-resonant backgrounds as well as the effective second-order nonlinear susceptibility tensor, which is a function of the interfacial ($\chi^{(2)}_{surface}$) and bulk ($\chi^{(3)}$) contributions, respectively. Equation 1 takes into account the $\chi^{(3)}$ contributions, which can be substantial for some charged lipid systems. It should be noted that previous studies have reported that high salt concentrations can affect lipid SFG spectra due to $\chi^{(3)}$ contributions based on electrostatic fields across monolayers.[50−52] Based on the code provided by previous work from the Geiger group, we have calculated electrostatics of our experiments and found a surface potential of 206 mV, which is far below the ~500 mV potentials used in previous studies that demonstrate large $\chi^{(3)}$ contributions.[50] Additionally, these recent studies by the Geiger group imply that at mM salt concentrations, water OH signals can be affected by $\chi^{(3)}$ effects.[52] This could be an issue for spectra collected in the amide-I region as an O−H bending mode at ~1650 cm^{-1} can potentially overlap with

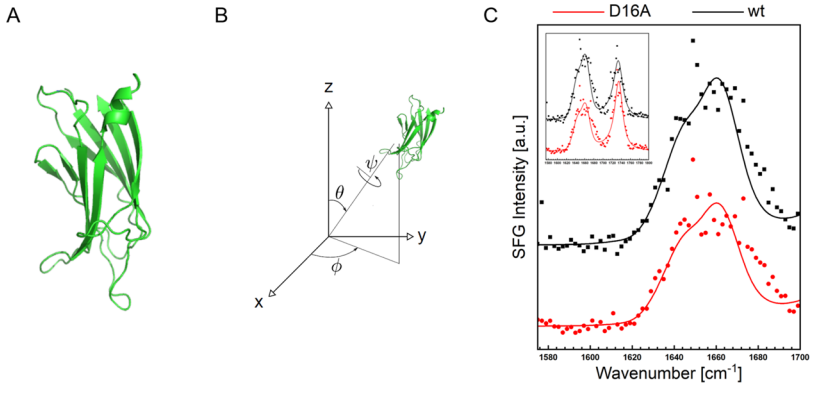

Figure 2. Structure of dysferlin C2A domain from PDB 4IQH (A). Coordinate system and Euler angles of the protein orientation in the laboratory frame (B). Optimal calculated spectra of the experimental ssp polarization for D16A (red) and DYSC2Awt (black), for a protein tilt angle $\Theta = 30 \pm 2°$ and a twist angle $\psi = 242 \pm 5°$ for wt and $\Theta = 31 \pm 4°$ and a twist angle $\psi = 237 \pm 9°$ for D16A mutant (C). The spectra are offset for clarity. The two-dimensional (2D)-RSS plot for the whole modeled spectral range (1575−1799 cm^{-1}) can be found in Figure S1.

https://dx.doi.org/10.1021/acs.jpcb.0c07143
J. Phys. Chem. B 2021, 125, 148−157

signal from a protein. However, recent work has demonstrated that at the ion concentrations used in these experiments we do not expect the O−H bending mode ∼1650 cm^{-1} and thus can leave it out of our spectral calculations.[53]

As a result of the experimental conditions used in this study, the $\chi^{(3)}$ contributions will be minimal and can be ignored. Therefore, eq 1 can be simplified to the following

$$\chi_{\text{eff}}^{(2)}(\omega) = \chi_{\text{NR}}^{(2)} + \sum_q \frac{A_q}{\omega - \omega_q + i\Gamma_q} \tag{2}$$

where Γ_q, A_q, and ω_q are the full width at half-maximum (FWHM), amplitude, and resonant frequency of the qth vibrational mode, respectively.

SFG Spectral Simulations. The spectral calculation is based on the formalism described in ref 54. In short, we construct a one-exciton Hamiltonian for the backbone amide groups in the protein, with a single local-mode frequency (i.e., assuming that, on average, all amide groups are hydrogen-bonded equally) and couplings that are modeled differently for nearest- and non-nearest-neighbor amide groups. The nearest-neighbor interactions, dominated by through-bond effects, are modeled using a parameterized map of an *ab initio* calculation with the 6-31G+(d) basis set and the B3LYP functional, which gives the coupling as a function of the dihedral angle.[55,56] The non-nearest-neighbor interactions, dominated by through-space effects, are modeled using the transition-dipole coupling model.[57] The Hamiltonian is then diagonalized to obtain the system's eigenvalues and eigenvectors, from which the spectroscopic response is calculated. Because the ssp spectrum includes a lipid peak, it was necessary to explicitly include this peak, as it, through constructive and destructive interference, influences the spectral shape in the amide-I region (1600−1700 cm^{-1}). We thus included a Lorentzian peak next to the amide-I peak, at 1708 cm^{-1} for the C═O groups that are present in the lipid headgroups.[32,54] To account for the azimuthal isotropy of the proteins at the interface, we average the Euler angle ϕ (see Figure 2) from 0 to 2π. We performed a grid search over the other two Euler angles, Θ and ψ, to find the minimum in the residual sum of squares (RSS) between the calculated and experimental spectra in the ssp polarization combination (using a single, overall scaling factor). In total, we calculated ∼10 000 spectra for this, varying Θ from 0 to 180°, and ψ from 0 to 360°, both with a resolution of 2.5°. We then performed a Levenberg−Marquardt least-squares fit in Θ and ψ near the RSS minimum to obtain the optimal angles (see the Results and Discussion section), taking into account the experimental errors on the datapoints. The errors on the fit parameters and the correlation matrix of this fit (plotted in Figure 2) can be found in Tables S3 and S4 in the Supporting Information. We model the local-field corrections as described in ref 58, for which we have assumed the refractive index of a lipid membrane for the layer above the interface, using the dispersion relation reported in ref 59 (leading to $n_{1,\text{SF}} = 1$, $n_{1,\text{VIS}} = 1$, and $n_{1,\text{IR}} = 1.18$ at the employed frequencies of ∼489, 532, and ∼6100 nm for the SF, VIS, and IR fields, respectively), the refractive index typical for bulk protein solutions[60] for the interfacial refractive indices (leading to $n_i = 1.47$ at all frequencies because the dispersion is almost negligible for proteins[61]), and the refractive index of bulk H_2O[62] for the layer below the surface (leading to $n_{2,\text{SF}} = 1.34$, $n_{2,\text{VIS}} = 1.34$, and $n_{2,\text{IR}} = 1.27$). An optimal match between calculations and experiment was found for a central frequency (the gas-phase frequency minus an overall frequency shift due to hydrogen bonding) of 1651 cm^{-1}, which is in line with previous calculations using the same method,[63] and a Lorentzian width of 5 cm^{-1}, which is in line with the experimentally determined line width of the IR beam.

RESULTS AND DISCUSSION

Many proteins that possess C2 domains, including dysferlin, bind membranes in a calcium-dependent manner via conserved aspartic acids in the binding loops combined with hydrophobic residues also at the binding loop, insert into the lipid bilayer of membranes. Binding is dependent on anionic lipids, such as phosphatidylserine, in the membrane.[17,19] The docking of the binding loops causes lipid clustering and spontaneous curvature change of the membrane, facilitating membrane fusion and exocytosis.[15,64] However, mutations to the binding loops reduce calcium sensitivity and ability of the domain to bind and interact with lipids.[17,19] Previous studies suggest that C2 domains are capable of altering the packing of lipid vesicles.[17,19] Specifically, dysferlin C2A has been found to alter the Laurdan signal in a dose-dependent manner, while the D16A mutation displayed significantly attenuated activity regardless of the presence of calcium.[19] However, analysis of sedimentation assay results indicates that D16A mutations still bind to vesicles composed of anionic lipids.[17] These two studies suggest that dysferlin C2A binding to lipid vesicles containing anionic lipids alters the packing of the lipids in the vesicle, while D16A binds to lipids but does not alter the packing of the lipids in the vesicle.

To observe protein−lipid binding, we probed changes in surface pressure at a model membrane surface. Initially, a well-ordered, lipid monolayer (in a liquid-expanded phase) was constructed at an air−water interface. The liquid-expanded phase was confirmed by a surface pressure measured to be 12 mN/m (Figure 1; traces I and IV).[29,30,35] The binding rate differences between DYSwt and D16A to a lipid monolayer were observed by tracking the relative changes in surface pressure with respect to time, following injection of proteins into the subphase and interaction with the lipid monolayer (Figure 1; traces II and V). Sedimentation assays have demonstrated that both DYSwt and D16A bind mixed phosphatidylserine and phosphatidylcholine vesicles.[19] However, substantially more binding was observed for DYSwt compared to that for the D16A variant. Therefore, we expect the D16A to bind to the membrane at a different rate than DYSwt.[17] Upon injection of DYSwt into the lipid membrane subphase, which includes 1 mM free Ca^{2+}, the surface pressure climbed until it reached steady state at approximately 19 mN/m (Figure 1; trace III). In comparison, for D16A, the time to pressure equilibrium of approximately 22 mN/m (Figure 1; trace VI) occurred approximately 20 times faster. It is important to note that the change in surface pressure for lipid monolayer experiments is recorded even if the protein does not dock with the membrane and perform its biological function.[29,65] So, the faster increase in surface pressure tells us that the D16A mutant is driven to the lipid interface at a faster rate than the wild type. One possibility is that the D16A variant, substituting a negatively charged aspartic acid to a hydrophobic alanine residue, causes the binding loop to be more hydrophobic, which will increase the protein's affinity for the interface. Additionally, the D-to-A substitution reduces the negative charge on the binding loops of the C2A domain and thus reduces the need for calcium ions to form a bridge with an

https://dx.doi.org/10.1021/acs.jpcb.0c07143
J. Phys. Chem. B 2021, 125, 148−157

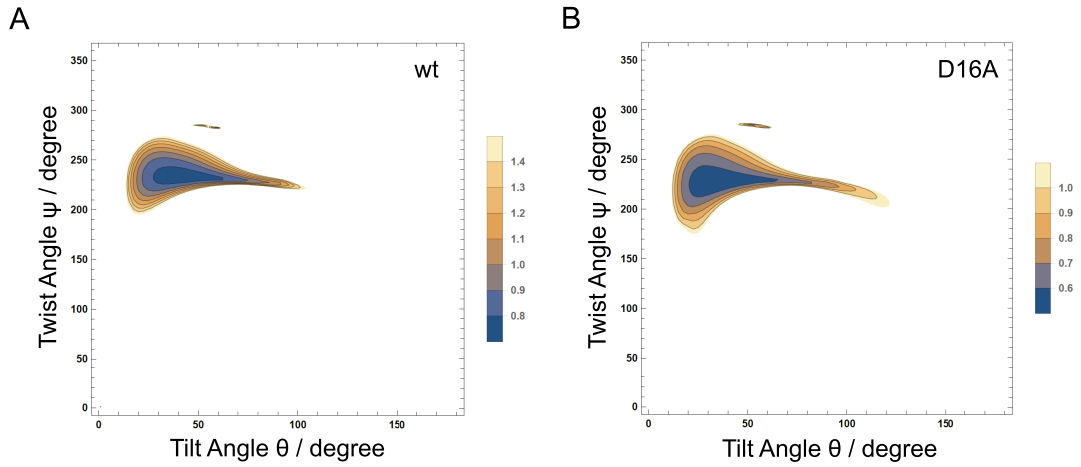

Figure 3. Error-weighted two-dimensional residual sum-of-squares (2D-RSS) plots of the amide-I and carbonyl (1575−1799 cm^{-1}) regions composed of ∼10 000 spectral calculations at a Θ and ψ resolution of 2.5° that indicates that the experimental spectra can only be modeled well for a specific range of protein orientations. In the white area, the error-weighted RSS is more than twice the minimal error-weighted RSS value (0.7 for wt and 0.5 for D16A). The 2D-RSS plots are for (A) wild-type dysferlin protein (wt) and (B) D16A mutant interacting with a DPPS and DPPC lipid monolayer.

anionic lipid while also reducing the overall repulsion forces between the anionic aspartic acids in the C2A domain and dDPPS lipids.[14] This corroborates well with previous experimental work that reported a loss of calcium sensitivity for the D16A variant binding to lipids.[2] Overall, this surface pressure data suggest that the faster time to equilibrium for the D16A mutant compared to that for DYSwt is due to the loss of an anionic−anionic electrostatic interaction, typically bridged by calcium, between the lipid membrane and the dysferlin C2A domain.[2,17]

Following the construction of the lipid monolayer, we could then directly observe the orientations of DYSwt and D16A docked to a lipid membrane with SFG. The backbone of a protein possesses unique vibrational modes depending on order, hydrogen bonding, and folding.[66−68] Thus, peaks present within the amide-I vibrational band can be used to identify protein secondary structures and, due to the unique selection rules of SFG, also provide the specific orientation of the protein interacting with a lipid interface. Amide-I spectra collected at the lipid interface of the DYSwt and D16A are presented in Figure 2. Specifically, for DYSwt and D16A, we observe three major resonances near 1642, 1663, and 1675 cm^{-1}. The resonances 1642 and 1663 cm^{-1} can be assigned to a combination of turns and random structure of the C2A domain structure,[69] while the resonance near 1675 cm^{-1} can be assigned to the B_1/B_3 modes of an antiparallel β-sheet secondary structure, respectively.[29,69] Additionally, we also observe the resonance of the carbonyl peak of the lipid near 1727 cm^{-1}.[29,30,32,37]

However, one powerful characteristic of SFG is that the spectral contributions of individual protein secondary structures, folding motifs, and orientations will interfere in specific ways resulting in a complex vibrational spectrum. SFG has previously been used to study lipid monolayers at the air/water interface,[31−35,70−72] model lipid bilayers,[36,39,73,74] and small proteins and peptide interaction with each type of model membrane.[29,32,36,39−42,73−79] For small proteins and peptides, the direct analysis of SFG amide-I spectra by peak fitting vibrational spectra relating to the C═O of the amide backbone can provide information about the orientation and structure.[41,80,81] However, since the DYSwt and D16A have complex domain structures, which leads to spectral convolution and interference, it is not possible to obtain unambiguous information about the protein conformation by direct spectral feature identification and fitting. To solve this problem, utilizing the full structural information within the SFG spectra, we have developed a framework for calculating theoretical SFG spectra from protein data bank (PDB)[54,82] and molecular dynamics structure files.[37,63,83−87] We have previously used this method to study the F domain of otoferlin.[65] Thus, spectra for this study were calculated from PDB models. Furthermore, by calculating spectra for different protein orientations to the surface normal and subsequently matching experimental and calculated spectra for various different orientations, the surface binding geometry can be determined.

Since the D16A variant does not have a solved crystal structure, we used the DYSwt domain structure because the difference is one amino acid point mutation in the binding loop.[2,17,22] Figure 2 shows the theoretical SFG spectra calculated for the crystal structure dysferlin C2A domain (PDB 4IQH) for tilt angles Θ = 30 ± 2 and 31 ± 4° and twist angles ψ = 242 ± 5 and 237 ± 9° for the DYSwt and D16A, respectively. Besides the absolute intensity and orientation, no adjustable parameters were used to match the calculated spectra to the experimental data. The calculations match the experimental spectral features very well (RSS < 0.7 for DYSwt and RSS < 0.5 for D16A; see Figure 3A,B), with main resonances near 1645, 1663, and 1675 cm^{-1}. Importantly, the relative intensities of the ssp spectra match the experimental data. The agreement of experimental and calculated spectra clearly indicates that both DYSwt and D16A maintain folded structures close to their native state when docking with a lipid monolayer.

Next, we determine the uniqueness of the spectral match for the set of tilt and twist angles for each of the domains, DYSwt and D16A. The orientation of each of the DYSwt and D16A domains was determined by a systematic grid search using varied tilt and twist angles. The RSS values were determined by comparing a total of ∼10 000 calculated spectra with the experimental spectra collected. The results of the search are summarized in Figure 3A,B. The 2D-RSS plots of each domain

https://dx.doi.org/10.1021/acs.jpcb.0c07143
J. Phys. Chem. B 2021, 125, 148−157

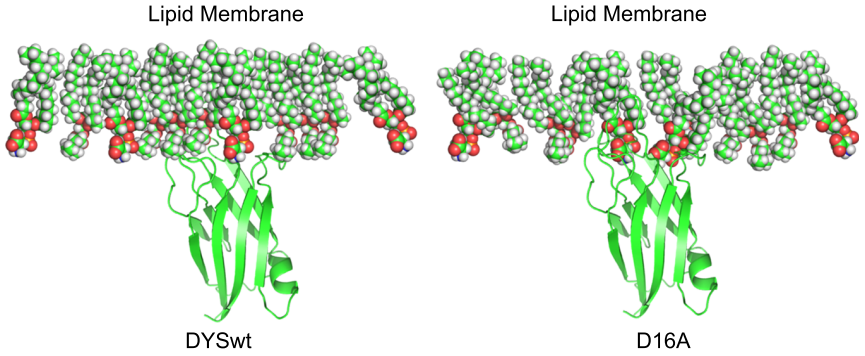

Figure 4. Dysferlin C2A wild type adopts a similar tilt angle to the membrane surface normal compared to the D16A mutant. The wild type "clusters" the lipid while inserting its binding loops into the membrane headgroup (left) but the mutant version, D16A, does not induce clustering to the same degree as the wild type.

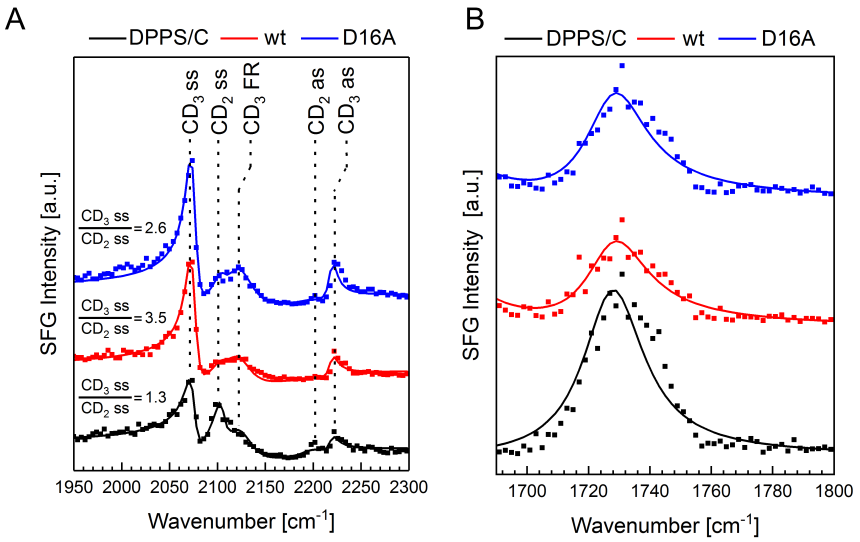

Figure 5. CD region (left) and carbonyl peak (right) ssp polarization combination of SFG spectrum of a 75% d62-DPPC and 25% d62-DPPS lipid monolayer before the injection (black) of protein and after 4 h of interaction of wt (red) and D16A (blue). Spectra are offset for clarity, and representative spectra are plotted from each type of protein experiment.

show one region with a protein orientation that results in a significant match between theory and experiment. The orientation of the DYSwt and D16A with respect to the normal of the lipid monolayer is shown in Figure 4. These tilt angles suggest that both DYSwt and D16A are docked in an orientation such that the β-sandwich structure is upright with the binding loops in contact with the membrane. This observed lipid binding geometry is similar to previous simulations that report that synaptotagmin 1's C2A domain also orients at the membrane interface at a tilt angle of 37.1 ± 9.5°.[88] However, the tilt angles of the C2 domains of synaptotagmin have also been proposed to adopt other angles in an apparently calcium-sensitive manner.[64]

Altogether, the amide-I calculated spectra and 2D-RSS plots suggest that, in the presence of anionic lipids, the DYSwt and D16A domains have the same orientation ($\ominus$ = 30 ± 2 and 31 ± 4°) to the surface normal of a lipid membrane. Next, to further investigate the necessity of anionic lipids in the lipid membrane, we compared the 2D-RSS plots of DYSwt with a membrane composed of 25% PS lipids and a membrane with 100% PC lipids. We found that the DYSwt domain adsorbs to the 100% PC lipid membrane with an optimal angle of $\ominus$ = 21 ± 1° to the surface normal (see the SI section). While the optimal calculated orientation of the DYSwt protein is not very different between the two lipid membranes, the 2D-RSS plot of the 100% PC lipid membrane suggests that DYSwt can adopt a myriad of different orientations (see the SI section), especially when we compare the 2D-RSS for the 100% PC to the 25% PS lipid membrane (Figure 3A) for the same protein (DYSwt). The result of the DYSwt having a 2D-RSS plot with many different orientations suggests that the protein is at the lipid membrane interface of 100% PC but does not dock with the membrane. This is supported by the sedimentation assays that do not show dysferlin C2A in the pellet of 100% PC vesicles; in this case, only the bound protein will be pulled into the pellet and out of the supernatant.[17] So, this leads to the next question we investigated: how does the DYSwt and D16A affect the lipid packing and structure of the lipid membranes upon docking?

To identify how a mutation affects the protein's ability to manipulate lipid membranes, we collected additional SFG spectra of the lipid monolayer both before (Figure 1; traces I and IV) and after (Figure 1; traces III and VI) the DYSwt and the D16A variant were allowed to interact for 4 h. We observed vibrational modes related to the lipid headgroup before and after adsorption of DYSwt and D16A by tracking a change in amplitude of the carbonyl peak near 1730 cm^{-1} (Figure 5). When a lipid membrane is disrupted by inserting itself into the

https://dx.doi.org/10.1021/acs.jpcb.0c07143
J. Phys. Chem. B 2021, 125, 148−157

Table 1. CD Region and Carbonyl Lipid Region ssp Polarization SFG Fitting Results of Dysferlin C2A Wild Type (DYSC2Awt) and D16A Mutant Interacting with a 1:3 Molar Ratio d62-DPPS and d62-DPPC Lipid Monolayer

	A_{NR}	φ_{NR}	ω_n (cm^{-1})	Γ_n (cm^{-1})	A_n
dDPPS/C	0.0021	2.80	2075	12.44	0.0161
			2105	12.73	0.0095
			2127	39.86	0.0557
			2195	35.68	−0.0139
	0.032	4.91	2219	10.86	−0.0037
			1727	24.18	0.841
dDPPS/C + DYSC2Awt	0.0021	2.80	2075	12.44	0.0260
			2105	12.73	0.0021
			2127	39.86	0.0490
			2195	35.68	−0.0046
	0.032	4.91	2219	10.86	−0.0061
			1727	24.18	0.500
dDPPS/C	0.0021	2.80	2075	12.44	0.0244
			2105	12.73	0.0167
			2127	39.86	0.0768
			2195	35.68	−0.0315
	0.032	4.91	2219	10.86	−0.0081
			1727	24.18	0.953
dDPPS/C + DYSC2A D16A	0.0021	2.80	2075	12.44	0.0438
			2105	12.73	0.0063
			2127	39.86	0.0836
			2195	35.68	−0.0115
	0.032	4.91	2219	10.86	−0.0164
			1727	24.18	0.595

lipid interface, a decrease in the amplitude of the lipid carbonyl peak will be observed.[29,37] Notably, there is a decrease in the carbonyl peak amplitude after adsorption and docking of each protein. We observed decreases of 41 ± 4 and 38 ± 5% for DYSwt and D16A, respectively, thereby suggesting that the binding loops of both proteins, DYSwt and D16A, insert into the lipid headgroups of the model cell lipid membrane.

We can further observe the lipid monolayer by using lipids with isotopically labeled acyl chains, which provided a way to isolate the molecular vibrations of the lipid monolayers from CH modes present within the protein. SFG spectra for the different proteins interacting with the lipid monolayer can be found in Figure 5, and SFG fitting parameters for the CD spectrum and the carbonyl peak are found in Table 1. Spectra collected before the injection of protein into the subphase contain resonances near 2075, 2100, 2125, 2200, 2225, and 1730 cm^{-1} assigned to the CD_3 symmetric, CD_2 symmetric, CD_3 Fermi resonance, CD_2 asymmetric, CD_3 asymmetric vibrations, and carbonyl peak, respectively.[29]

For both cases, following adsorption of DYSwt and D16A, the amplitudes of the vibrational modes corresponding to CD_3 groups increased, while the amplitudes of the CD_2 groups decreased. We can quantify the increase in lipid order by taking the ratio of the methyl and methylene symmetric stretches before and after the protein adsorption. A ratio value that increases after protein adsorption suggests that the lipid monolayer packs together tighter.[29,30,32] For the dysferlin C2A wild-type adsorption and interaction (Figure 5; red trace), the ratio of the CD_3 and CD_2 symmetric intensities increases by 170% from 1.3 ± 0.2 to 3.5 ± 0.1. This suggests that the lipids in the already ordered monolayer are clustering together tighter. Following adsorption of D16A (Figure 5; blue trace), the ratio increases by 120%, from 1.3 ± 0.2 to 2.6 ± 0.1. What is even more convincing is when we compare the D16A acyl chain order ratio of the 25% PS lipid membrane to the DYSwt 100% PC lipid membrane (see the SI section) case, 1.4−2.7, the percent increase is the same. So, since the DYSwt does not interact with PC lipids, then the fact that the order ratio is similar suggests that the D16A mutant is inactive and this ratio increase is just due to protein at the interface of a constant area trough, which has been previously observed.[29] Combined, this suggests that the D16A mutation causes the C2A domain to cluster lipids less effectively compared to DYSwt.

CONCLUSIONS

Combined, the experiments presented here illustrate three points. First, a mutation within the lipid binding loop of dysferlin C2A does not affect the lipid binding geometry of the protein. However, the point mutation does change the calcium sensitivity of the binding process. Finally, while dysferlin C2A clusters lipids after docking, the D16A variant is unable to cluster the lipids as effectively. The ability to cluster lipids while changing the curvature of a membrane is important as it is one of the initial steps facilitating exocytosis and endocytosis. Since dysferlin facilitates the resealing of muscle cell membrane tears by vesicle fusion, we have investigated protein docking ability and vesicle structural changes that occur during the first important step in vesicle fusion. This study provides a direct observation of the initial dysferlin lipid binding and clustering of lipids, in which mutations of this domain have been linked to various forms of recessive muscular dystrophy.

ASSOCIATED CONTENT

Supporting Information

The Supporting Information is available free of charge at https://pubs.acs.org/doi/10.1021/acs.jpcb.0c07143.

Amino acid sequence of dysferlin C2A, 2D-RSS plot for the modeled SFG spectra, amide region ssp polarization

https://dx.doi.org/10.1021/acs.jpcb.0c07143
J. Phys. Chem. B 2021, 125, 148−157

SFG fitting results, surface pressure versus time of protein adsorption, SFG spectrum of a pure dDPPC lipid monolayer, SFG fitting results of dysferlin C2A wild type at the lipid interface, amide SFG spectra and optimal fits, error-weighted two-dimensional residual sum-of-squares (2D-RSS) plots, and various scenarios for the dysferlin C2A wild type of calculated SFG spectra (PDF)

AUTHOR INFORMATION

Corresponding Authors

Colin P. Johnson − *Department of Biochemistry and Biophysics, Oregon State University, Corvallis, Oregon 97331, United States;* orcid.org/0000-0002-6783-2835; Email: Colin.Johnson@oregonstate.edu

Joe E. Baio − *School of Chemical, Biological, and Environmental Engineering, Oregon State University, Corvallis, Oregon 97331, United States;* orcid.org/0000-0002-9692-689X; Email: joe.baio@oregonstate.edu

Authors

Thaddeus W. Golbek − *Department of Chemistry, Aarhus University, 8000 Aarhus C, Denmark*

Shauna C. Otto − *Department of Biochemistry and Biophysics, Oregon State University, Corvallis, Oregon 97331, United States*

Steven J. Roeters − *Department of Chemistry, Aarhus University, 8000 Aarhus C, Denmark;* orcid.org/0000-0003-3238-2181

Tobias Weidner − *Department of Chemistry, Aarhus University, 8000 Aarhus C, Denmark;* orcid.org/0000-0002-7083-7004

Complete contact information is available at: https://pubs.acs.org/10.1021/acs.jpcb.0c07143

Notes

The authors declare no competing financial interest.

ACKNOWLEDGMENTS

This work was supported by John C. Erkkila, M.D., Endowment for Health and Human Performance, NIH National Institute of Deafness and Other Communication Disorders (NIDCD) Grant R01DC014588 to C.P.J. and the National Science Foundation award #1905091. T.W.G. would like to thank the Lundbeck Foundation (postdoc grant R322-2019-2461). S.J.R. acknowledges the Lundbeck Foundation for funding through fellowship grant R303-2018-349.

REFERENCES

(1) McNeil, P. L. Repairing a torn cell surface: make way, lysosomes to the rescue. *J. Cell Sci.* **2002**, *115*, 873.

(2) Fuson, K.; Rice, A.; Mahling, R.; Snow, A.; Nayak, K.; Shanbhogue, P.; Meyer, A. G.; Redpath, G. M. I.; et al. Alternate splicing of dysferlin C2A confers Ca2+-dependent and Ca2+-independent binding for membrane repair. *Structure* **2014**, *22*, 104−115.

(3) Emery, A. E. H.; Muntoni, F.; Quinlivan, R. C. M. Molecular Pathology. *Duchenne Muscular Dystrophy*; Oxford University Press: Oxford, 2015; pp 148−168.

(4) Han, R.; Campbell, K. P. Dysferlin and muscle membrane repair. *Curr. Opin. Cell Biol.* **2007**, *19*, 409−416.

(5) Hofhuis, J.; Bersch, K.; Büssenschütt, R.; Drzymalski, M.; Liebetanz, D.; Nikolaev, V. O.; Wagner, S.; Maier, L. S.; Gärtner, J.; et al. Dysferlin mediates membrane tubulation and links T-tubule biogenesis to muscular dystrophy. *J. Cell Sci.* **2017**, *130*, 841.

(6) Bansal, D.; Miyake, K.; Vogel, S. S.; Groh, S.; Chen, C.-C.; Williamson, R.; McNeil, P. L.; Campbell, K. P. Defective membrane repair in dysferlin-deficient muscular dystrophy. *Nature* **2003**, *423*, 168.

(7) Illa, I.; Serrano-Munuera, C.; Gallardo, E.; Lasa, A.; Rojas-García, R.; Palmer, J.; Gallano, P.; Baiget, M.; Matsuda, C.; et al. Distal anterior compartment myopathy: a dysferlin mutation causing a new muscular dystrophy phenotype. *Ann. Neurol.* **2001**, *49*, 130−134.

(8) Saito, H.; Suzuki, N.; Ishiguro, H.; Hirota, K.; Itoyama, Y.; Takahashi, T.; Aoki, M. Distal anterior compartment myopathy with early ankle contractures. *Muscle Nerve* **2007**, *36*, 525−527.

(9) Essen, L.-O.; Perisic, O.; Cheung, R.; Katan, M.; Williams, R. L. Crystal structure of a mammalian phosphoinositide-specific phospholipase Cδ. *Nature* **1996**, *380*, 595.

(10) Sutton, R. B.; Davletov, B. A.; Berghuis, A. M.; Sudhof, T. C.; Sprang, S. R. Structure of the first C2 domain of synaptotagmin I: A novel Ca2+/phospholipid-binding fold. *Cell* **1995**, *80*, 929−938.

(11) Pangršič, T.; Reisinger, E.; Moser, T. Otoferlin: a multi-C2 domain protein essential for hearing. *Trends Neurosci.* **2012**, *35*, 671−680.

(12) Corbalan-Garcia, S.; Gómez-Fernández, J. C. Signaling through C2 domains: more than one lipid target. *Biochim. Biophys. Acta, Biomembr.* **2014**, *1838*, 1536−1547.

(13) Cooper, S. T.; McNeil, P. L. Membrane repair: mechanisms and pathophysiology. *Physiol. Rev.* **2015**, *95*, 1205−1240.

(14) Cho, W.; Stahelin, R. V. Membrane binding and subcellular targeting of C2 domains. *Biochim. Biophys. Acta, Mol. Cell Biol. Lipids* **2006**, *1761*, 838−849.

(15) Hui, E.; Johnson, C. P.; Yao, J.; Dunning, F. M.; Chapman, E. R. Synaptotagmin-mediated bending of the target membrane is a critical step in Ca2+-regulated fusion. *Cell* **2009**, *138*, 709−721.

(16) Hui, E.; Bai, J.; Chapman, E. R. Ca2+-triggered simultaneous membrane penetration of the tandem C2-domains of synaptotagmin I. *Biophys. J.* **2006**, *91*, 1767−1777.

(17) Abdullah, N.; Padmanarayana, M.; Marty, N. J.; Johnson, C. P. Quantitation of the calcium and membrane binding properties of the C2 domains of dysferlin. *Biophys. J.* **2014**, *106*, 382−389.

(18) Davis, D. B.; Doherty, K. R.; Delmonte, A. J.; McNally, E. M. Calcium-sensitive phospholipid binding properties of normal and mutant ferlin C2 domains. *J. Biol. Chem.* **2002**, *277*, 22883−22888.

(19) Marty, N. J.; Holman, C. L.; Abdullah, N.; Johnson, C. P. The C2 domains of otoferlin, dysferlin, and myoferlin alter the packing of lipid bilayers. *Biochemistry* **2013**, *52*, 5585−5592.

(20) McNeil, P. L.; Steinhardt, R. A. Plasma membrane disruption: repair, prevention, adaptation. *Annu. Rev. Cell Dev. Biol.* **2003**, *19*, 697−731.

(21) Lek, A.; Evesson Frances, J.; Sutton, R. B.; North Kathryn, N.; Cooper Sandra, T. Ferlins: Regulators of vesicle fusion for auditory neurotransmission, receptor trafficking and membrane repair. *Traffic* **2012**, *13*, 185−194.

(22) Padmanarayana, M.; Hams, N.; Speight, L. C.; Petersson, E. J.; Mehl, R. A.; Johnson, C. P. Characterization of the lipid binding properties of otoferlin reveals specific interactions between PI (4, 5) P2 and the C2C and C2F domains. *Biochemistry* **2014**, *53*, 5023−5033.

(23) Brockman, H. Lipid Monolayers: Why use half a membrane to characterize protein-membrane interactions? *Curr. Opin. Struct. Biol.* **1999**, *9*, 438−443.

(24) Lambert, A. G.; Davies, P. B.; Neivandt, D. J. Implementing the theory of sum frequency generation vibrational spectroscopy: a tutorial review. *Appl. Spectrosc. Rev.* **2005**, *40*, 103−145.

(25) McGilp, J. Second Harmonic and Sum Frequency Generation. *Epioptics*; Springer, 1995; pp 183−206.

(26) Shen, Y.-R. *The Principles of Nonlinear Optics*; Wiley-Interscience: New York, 1984; Vol. 1, p 575.

(27) Wang, H.-F.; Velarde, L.; Gan, W.; Fu, L. Quantitative sum-frequency generation vibrational spectroscopy of molecular surfaces

and interfaces: lineshape, polarization, and orientation. *Annu. Rev. Phys. Chem.* **2015**, *66*, 189−216.
(28) Wang, H.-F.; Gan, W.; Lu, R.; Rao, Y.; Wu, B.-H. Quantitative spectral and orientational analysis in surface sum frequency generation vibrational spectroscopy (SFG-VS). *Int. Rev. Phys. Chem.* **2005**, *24*, 191−256.
(29) Golbek, T. W.; Franz, J.; Fowler, J. E.; Schilke, K. F.; Weidner, T.; Baio, J. E. Identifying the selectivity of antimicrobial peptides to cell membranes by sum frequency generation spectroscopy. *Biointerphases* **2017**, *12*, No. 02D406.
(30) Franz, J.; Bereau, T.; Pannwitt, S.; Anbazhagan, V.; Lehr, A.; Nubbemeyer, U.; Dietz, U.; Bonn, M.; Weidner, T.; et al. Nitrated fatty acids modulate the physical properties of model membranes and the structure of transmembrane proteins. *Chem. - Eur. J.* **2017**, *23*, 9690−9697.
(31) Franz, J.; Lelle, M.; Peneva, K.; Bonn, M.; Weidner, T. SAP(E) − a cell-penetrating polyproline helix at lipid interfaces. *Biochim. Biophys. Acta, Biomembr.* **2016**, *1858*, 2028−2034.
(32) Schach, D. K.; Rock, W.; Franz, J.; Bonn, M.; Parekh, S. H.; Weidner, T. Reversible activation of a cell-penetrating peptide in a membrane environment. *J. Am. Chem. Soc.* **2015**, *137*, 12199−12202.
(33) Mauri, S.; Pandey, R.; Rzeznicka, I.; Lu, H.; Bonn, M.; Weidner, T. Bovine and human insulin adsorption at lipid monolayers: a comparison. *Front. Phys.* **2015**, *3*, No. 51.
(34) Watry, M. R.; Tarbuck, T. L.; Richmond, G. L. Vibrational sum-frequency studies of a series of phospholipid monolayers and the associated water structure at the vapor/water interface. *J. Phys. Chem. B* **2003**, *107*, 512−518.
(35) Ma, G.; Allen, H. C. DPPC langmuir monolayer at the air−water interface: probing the tail and head groups by vibrational sum frequency generation spectroscopy. *Langmuir* **2006**, *22*, 5341−5349.
(36) Chen, X.; Wang, J.; Boughton, A. P.; Kristalyn, C. B.; Chen, Z. Multiple orientation of melittin inside a single lipid bilayer determined by combined vibrational spectroscopic studies. *J. Am. Chem. Soc.* **2007**, *129*, 1420−1427.
(37) Hennig, R.; Heidrich, J.; Saur, M.; Schmüser, L.; Roeters, S. J.; Hellmann, N.; Woutersen, S.; Bonn, M.; Weidner, T.; et al. IM30 triggers membrane fusion in cyanobacteria and chloroplasts. *Nat. Commun.* **2015**, *6*, No. 7018.
(38) Chen, X.; Clarke, M. L.; Wang, J.; Chen, Z. Sum frequency generation vibrational spectroscopy studies on molecular conformation and orientation of biological molecules at interfaces. *Int. J. Mod. Phys. B* **2005**, *19*, 691−713.
(39) Chen, X.; Chen, Z. SFG studies on interactions between antimicrobial peptides and supported lipid bilayers. *Biochim. Biophys. Acta, Biomembr.* **2006**, *1758*, 1257−1273.
(40) Ding, B.; Chen, Z. Molecular interactions between cell penetrating peptide pep-1 and model cell membranes. *J. Phys. Chem. B* **2012**, *116*, 2545−2552.
(41) Nguyen, K. T.; King, J. T.; Chen, Z. Orientation determination of interfacial β-sheet structures in situ. *J. Phys. Chem. B* **2010**, *114*, 8291−8300.
(42) Nguyen, K. T.; Le Clair, S. V.; Ye, S.; Chen, Z. Molecular interactions between magainin 2 and model membranes in situ. *J. Phys. Chem. B* **2009**, *113*, 12358−12363.
(43) Baio, J. E.; Weidner, T.; Baugh, L.; Gamble, L. J.; Stayton, P. S.; Castner, D. G. Probing the orientation of electrostatically immobilized protein G B1 by time-of-flight secondary ion spectrometry, sum frequency generation, and near-edge x-ray adsorption fine structure spectroscopy. *Langmuir* **2012**, *28*, 2107−2112.
(44) Baio, J. E.; Weidner, T.; Castner, D. G. Characterizing the Structure of Surface-Immobilized Proteins: A Surface Analysis Approach. *ACS Symp. Ser.* **2012**, *1120*, 761−779.
(45) Baio, J. E.; Weidner, T.; Ramey, D.; Pruzinsky, L.; Castner, D. G. Probing the orientation of electrostatically immobilized cytochrome c by time of flight secondary ion mass spectrometry and sum frequency generation spectroscopy. *Biointerphases* **2013**, *8*, No. 18.
(46) Duncan, S. L.; Larson, R. G. Comparing experimental and simulated pressure-area isotherms for DPPC. *Biophys. J.* **2008**, *94*, 2965−2986.
(47) Niño, M. R. R.; Sánchez, C. C.; Patino, J. M. R. Interfacial characteristics of β-casein spread films at the air−water interface. *Colloids Surf., B* **1999**, *12*, 161−173.
(48) Bain, C. D. Sum-Frequency vibrational spectroscopy of the solid/liquid interface. *J. Chem. Soc., Faraday Trans.* **1995**, *91*, 1281−1296.
(49) Moore, F. G.; Becraft, K. A.; Richmond, G. L. Challenges in interpreting vibrational sum frequency spectra: deconvoluting spectral features as demonstrated in the calcium fluoride—water—sodium dodecylsulfate system. *Appl. Spectrosc.* **2002**, *56*, 1575−1578.
(50) Ohno, P. E.; Wang, H.-f.; Geiger, F. M. Second-order spectral lineshapes from charged interfaces. *Nat. Commun.* **2017**, *8*, No. 1032.
(51) Ohno, P. E.; Wang, H.-f.; Paesani, F.; Skinner, J. L.; Geiger, F. M. Second-order vibrational lineshapes from the air/water interface. *J. Phys. Chem. A* **2018**, *122*, 4457−4464.
(52) Reddy, S. K.; Thiraux, R.; Wellen Rudd, B. A.; Lin, L.; Adel, T.; Joutsuka, T.; Geiger, F. M.; Allen, H. C.; Morita, A.; Paesani, F. Bulk contributions modulate the sum-frequency generation spectra of water on model sea-spray aerosols. *Chem* **2018**, *4*, 1629−1644.
(53) Seki, T.; Sun, S.; Zhong, K.; Yu, C.-C.; Machel, K.; Dreier, L. B.; Backus, E. H. G.; Bonn, M.; Nagata, Y. Unveiling Heterogeneity of Interfacial Water through the Water Bending Mode. *J. Phys. Chem. Lett.* **2019**, *10*, 6936−6941.
(54) Roeters, S. J.; van Dijk, C. N.; Torres-Knoop, A.; Backus, E. H. G.; Campen, R. K.; Bonn, M.; Woutersen, S. Determining in situ protein conformation and orientation from the amide-I sum-frequency generation spectrum: theory and experiment. *J. Phys. Chem. A* **2013**, *117*, 6311−6322.
(55) Gorbunov, R. D.; Kosov, D. S.; Stock, G. Ab initio-based exciton model of amide I vibrations in peptides: Definition, conformational dependence, and transferability. *J. Chem. Phys.* **2005**, *122*, No. 224904.
(56) Hamm, P.; Zanni, M. *Concepts and Methods of 2D Infrared Spectroscopy*; Cambridge University Press, 2011.
(57) Krimm, S.; Bandekar, J. Vibrational Spectroscopy and Conformation of Peptides, Polypeptides, and Proteins. *Adv. Protein Chem.*; Elsevier, 1986; Vol. *38*, pp 181−364.
(58) Zhuang, X.; Miranda, P. B.; Kim, D.; Shen, Y. R. Mapping molecular orientation and conformation at interfaces by surface nonlinear optics. *Phys. Rev. B: Condens. Matter Mater. Phys.* **1999**, *59*, 12632−12640.
(59) Sultanova, N. G.; Kasarova, S.; Nikolov, I. Dispersion properties of optical polymers. *Acta Phys. Pol., A* **2009**, *116*, 585−587.
(60) Hand, D. B. The refractivity of protein solutions. *J. Biol. Chem.* **1935**, *108*, 703−707.
(61) Bucciarelli, A.; Mulloni, V.; Maniglio, D.; Pal, R.; Yadavalli, V.; Motta, A.; Quaranta, A. A comparative study of the refractive index of silk protein thin films towards biomaterial based optical devices. *Opt. Mater.* **2018**, *78*, 407−414.
(62) Hale, G. M.; Querry, M. R. Optical constants of water in the 200-nm to 200-μm wavelength region. *Appl. Opt.* **1973**, *12*, 555−563.
(63) Schmüser, L.; Roeters, S.; Lutz, H.; Woutersen, S.; Bonn, M.; Weidner, T. Determination of absolute orientation of protein α-helices at interfaces using phase-resolved sum frequency generation spectroscopy. *J. Phys. Chem. Lett.* **2017**, *8*, 3101−3105.
(64) Vermaas, J. V.; Tajkhorshid, E. Differential membrane binding mechanics of synaptotagmin isoforms observed in atomic detail. *Biochemistry* **2017**, *56*, 281−293.
(65) Golbek, T. W.; Padmanarayana, M.; Roeters, S. J.; Weidner, T.; Johnson, C. P.; Baio, J. E. Otoferlin C2F domain-induced changes in membrane structure observed by sum frequency generation. *Biophys. J.* **2019**, *117*, No. 1820.
(66) Barth, A. Infrared spectroscopy of proteins. *Biochim. Biophys. Acta, Bioenerg.* **2007**, *1767*, 1073−1101.

https://dx.doi.org/10.1021/acs.jpcb.0c07143
J. Phys. Chem. B 2021, 125, 148−157

(67) Kong, J.; Yu, S. Fourier transform infrared spectroscopic analysis of protein secondary structures. *Acta Biochim. Biophys. Sin.* **2007**, *39*, 549−559.
(68) Singh, B. R. *Infrared Analysis of Peptides and Proteins*; American Chemical Society, 2000.
(69) Ye, S.; Nguyen, K. T.; Clair, S. V. L.; Chen, Z. In situ molecular level studies on membrane related peptides and proteins in real time using sum frequency generation vibrational spectroscopy. *J. Struct. Biol.* **2009**, *168*, 61−77.
(70) Liljeblad, J. F.; Bulone, V.; Tyrode, E.; Rutland, M. W.; Johnson, C. M. Phospholipid monolayers probed by vibrational sum frequency spectroscopy: instability of unsaturated phospholipids. *Biophys. J.* **2010**, *98*, L50−L52.
(71) Liljeblad, J. F. D.; Bulone, V.; Rutland, M. W.; Johnson, C. M. Supported phospholipid monolayers, the molecular structure investigated by vibrational sum frequency spectroscopy. *J. Phys. Chem. C* **2011**, *115*, 10617−10629.
(72) Maget-Dana, R. The monolayer technique: a potent tool for studying the interfacial properties of antimicrobial and membranelytic peptides and their interactions with lipid membranes. *Biochim. Biophys. Acta, Biomembr.* **1999**, *1462*, 109−140.
(73) Chen, X.; Wang, J.; Kristalyn, C. B.; Chen, Z. Real-time structural investigation of a lipid bilayer during its interaction with melittin using sum frequency generation vibrational spectroscopy. *Biophys. J.* **2007**, *93*, 866−875.
(74) Wang, T.; Li, D.; Lu, X.; Khmaladze, A.; Han, X.; Ye, S.; Yang, P.; Xue, G.; He, N.; et al. Single lipid bilayers constructed on polymer cushion studied by sum frequency generation vibrational spectroscopy. *J. Phys. Chem. C* **2011**, *115*, 7613−7620.
(75) Rzeźnicka, I.; Pandey, R.; Schleeger, M.; Bonn, M.; Weidner, T. Formation of lysozyme oligomers at model cell membranes monitored with sum frequency generation spectroscopy. *Langmuir* **2014**, *30*, 7736−7744.
(76) Liu, Y.; Jasensky, J.; Chen, Z. Molecular interactions of proteins and peptides at interfaces studied by sum frequency generation vibrational spectroscopy. *Langmuir* **2012**, *28*, 2113−2121.
(77) Nguyen, K. T.; Soong, R.; lm, S.-C.; Waskell, L.; Ramamoorthy, A.; Chen, Z. Probing the spontaneous membrane insertion of a tail-anchored membrane protein by sum frequency generation spectroscopy. *J. Am. Chem. Soc.* **2010**, *132*, 15112−15115.
(78) Thennarasu, S.; Huang, R.; Lee, D.-K.; Yang, P.; Maloy, L.; Chen, Z.; Ramamoorthy, A. Limiting an antimicrobial peptide to the lipid−water interface enhances its bacterial membrane selectivity: a case study of MSI-367. *Biochemistry* **2010**, *49*, 10595−10605.
(79) Wang, J.; Buck, S. M.; Chen, Z. Sum frequency generation vibrational spectroscopy studies on protein adsorption. *J. Phys. Chem. B* **2002**, *106*, 11666−11672.
(80) Nguyen, K. T.; Le Clair, S. V.; Ye, S.; Chen, Z. Orientation Determination of Protein Helical Secondary Structures Using Linear and Nonlinear Vibrational Spectroscopy. *J. Phys. Chem. B* **2009**, *113*, 12169−12180.
(81) Liu, Y.; Tan, J.; Zhang, J.; Li, C.; Luo, Y.; Ye, S. Influenza A M2 transmembrane domain tunes its conformational heterogeneity and structural plasticity in the lipid bilayer by forming loop structures. *Chem. Commun.* **2018**, *54*, 5903−5906.
(82) Verreault, D.; Alamdari, S.; Roeters, S. J.; Pandey, R.; Pfaendtner, J.; Weidner, T. Ice-binding site of surface-bound type III antifreeze protein partially decoupled from water. *Phys. Chem. Chem. Phys.* **2018**, *20*, 26926−26933.
(83) Schach, D.; Globisch, C.; Roeters, S. J.; Woutersen, S.; Fuchs, A.; Weiss, C. K.; Backus, E. H. G.; Landfester, K.; Bonn, M.; et al. Sticky water surfaces: helix−coil transitions suppressed in a cell-penetrating peptide at the air-water interface. *J. Chem. Phys.* **2014**, *141*, No. 22D517.
(84) Lu, H.; Lutz, H.; Roeters, S. J.; Hood, M. A.; Schäfer, A.; Muñoz-Espí, R.; Berger, R.; Bonn, M.; Weidner, T. Calcium-induced molecular rearrangement of peptide folds enables biomineralization of vaterite calcium carbonate. *J. Am. Chem. Soc.* **2018**, *140*, 2793−2796.
(85) Baio, J. E.; Zane, A.; Jaeger, V.; Roehrich, A. M.; Lutz, H.; Pfaendtner, J.; Drobny, G. P.; Weidner, T. Diatom mimics: directing the formation of biosilica nanoparticles by controlled folding of lysine-leucine peptides. *J. Am. Chem. Soc.* **2014**, *136*, 15134−15137.
(86) Lutz, H.; Jaeger, V.; Berger, R.; Bonn, M.; Pfaendtner, J.; Weidner, T. Biomimetic growth of ultrathin silica sheets using artificial amphiphilic peptides. *Adv. Mater. Interfaces* **2015**, *2*, No. 1500282.
(87) Harrison, E. T.; Weidner, T.; Castner, D. G.; Interlandi, G. Predicting the orientation of protein G B1 on hydrophobic surfaces using monte carlo simulations. *Biointerphases* **2016**, *12*, No. 02D401.
(88) Osterberg, J. R.; Chon, N. L.; Boo, A.; Maynard, F. A.; Lin, H.; Knight, J. D. Membrane docking of the synaptotagmin 7 C2A domain: electron paramagnetic resonance measurements show contributions from two membrane binding loops. *Biochemistry* **2015**, *54*, 5684−5695.

https://dx.doi.org/10.1021/acs.jpcb.0c07143
J. Phys. Chem. B 2021, 125, 148−157